Acta Cryst. (1988). B44, 183–187

Screened Precession Method for Area Detectors*

BY STEVEN L. EDWARDS,†‡ CHRIS NIELSEN§ AND NGUYEN HUU XUONG‡§¶

Departments of Chemistry, Physics and Biology, University of California, San Diego, La Jolla, California 92093, *USA*

(*Received* 4 *August* 1987; *accepted* 6 *November* 1987)

Abstract

A method is presented in which the features of a Buerger-type mechanical precession camera can be simulated using an electronic area detector and a three-circle automated goniostat. The resulting display as viewed on a video monitor is very much like a conventional precession photograph. The detector is stationary which causes a distortion that is negligible for precession angles less than 10°. The virtue of this new method is that a precession image may be collected very fast and the intensities of the reflections when displayed are already digitized. The usefulness of these features is presented through two familiar tasks: the determination of a new protein crystal space group and the evaluation of a heavy-atom derivative.

Introduction

Area detectors for protein crystallography are increasing in popularity because of their ability to make accurate measurements on many reflections simultaneously. The successful use of area detectors to solve crystal structures is well documented (Xuong, Sullivan, Nielsen & Hamlin, 1985; Poulos, Finzel & Howard, 1987; Huber *et al.*, 1987). We report here the use of an area detector in the preliminary steps of protein structure solution: determining space groups and evaluating heavy-atom derivatives.

These steps are normally performed on a standard precession camera (Buerger, 1964). The great virtue of this camera is that it reproduces separate layers of reciprocal space so that indexing of reflections is straightforward. We sought after this simplicity in devising a method to simulate screened precession photography using an electronic area detector. The two elements needed to accomplish this were precession motion of the crystal, driven by goniostat stepper motors, and proper filtering of the digital display to produce an image like the familiar precession photograph. Unlike the precession camera in which the film holder precesses, the electronic area detector remains stationary. The effect of having the detector fixed is a minor distortion in the resulting display that is not noticeable when using a precession angle of less than 10°. This distortion has been described by Buerger because it results from the same geometry used on his prototype Mark I precession camera (Buerger, 1964, p. 6).

The precession motion is calculated by the application of trigonometry to set the three goniostat motors, ω, φ and χ, to appropriate values. This feature had already been implemented because of its usefulness in displaying the symmetry around the rotation axes of some crystal groups. We describe it briefly as follows.

Calculating motor values for precession

The precession action results from combined motions around the vertical and horizontal axes. Because of the geometry of a typical three-circle goniostat, the ω axis will always cause the crystal to be rotated around a true vertical axis. However, rotation of the crystal around a horizontal axis normal to the X-ray beam usually requires adjustments of ω, φ and χ simultaneously. This task has been programmed as a subroutine which we refer to as motor 3, an imaginary motor designed to rotate the crystal around a horizontal axis much as the spindle axis on a precession camera. We refer to the ω motor as motor 0; the other real motors, φ and χ, are assigned the motor numbers 1 and 2. The algorithm to calculate the precession motion of the crystal reduces to calculating the appropriate values for motor 3 and the ω motor so that the crystal axis of alignment is tilted from the direct beam by the desired precession angle, μ, and then rotated around the beam so that this axis describes a circle on the detector (see Fig. 1). This circle suggests that the values for the vertical axis (motor 0) and the horizontal axis (motor 3) may be derived from positions on the circle (see Fig. 2). The radius of this circle, R, can be expressed in terms of the distance from the detector to the crystal, D, and the precession angle, μ:

$$R = D \tan \mu.$$

* This work was supported by National Institute of Health grant RR 01644 to the UCSD Data Collection Resource for Protein Crystallography in addition to a special grant from the NSF Biological Instrument Program PCM-8400547 and a grant for low-temperature experimentation, DMB-8510860.

† Author to whom correspondence should be addressed.

‡ Department of Chemistry.

§ Department of Biology.

¶ Department of Physics.

0108-7681/88/020183-05$03.00

For calculation purposes, this is also the radius of the zero circle. In Fig. 2, progress of the precession is indicated by a vector which makes an angle of $n°$ with the starting position, straight up, and moves clockwise like the hand of a clock. The horizontal (Δx) and vertical (Δy) components of this vector correspond to motor 0 and motor 3 values and can be expressed as functions of the angular progress through the precession cycle by:

$$\Delta x = R \sin n° = D \tan \mu \sin n°,$$

$$\Delta y = R \cos n° = D \tan \mu \cos n°.$$

The motor 0 and motor 3 values may be expressed as functions of Δx and Δy:

$$\text{motor } 0 = \arctan (\Delta x/D) = \arctan (\tan \mu \sin n°),$$

$$\text{motor } 3 = \arctan (\Delta y/D) = \arctan (\tan \mu \cos n°).$$

In practice we divide the precession cycle up into 360 one-degree increments (n) and expose the crystal for a specified amount of time between each step. Smooth continuous precession motion is not possible here because only one goniostat motor may be driven at a time. The resulting image is therefore a composite of 360 images (a multiple exposure in the terms of conventional photography). We point out that the angular velocity of this calculated precession motion is essentially constant (albeit in discrete steps), in contrast to the mechanical camera which varies somewhat depending on the precession angle. Variation of the angular velocity necessitates the use of a more complex Lorentz factor which has been described (Waser, 1951; Buerger, 1964, p. 198). The more constant angular velocity of the calculated precession allows use of the simpler Lorentz factor (Buerger, 1964, p. 197, equation 24).

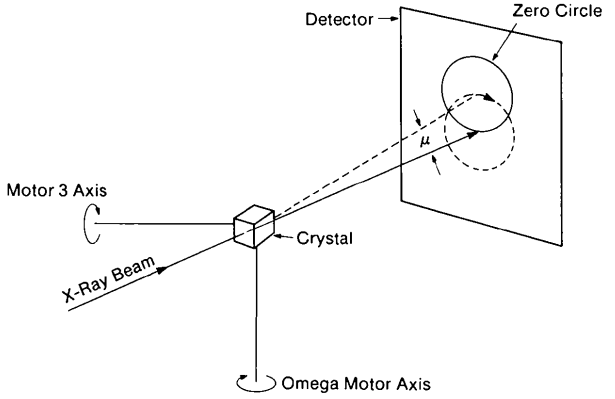

Fig. 1. Orientation of the imaginary motor (motor 3) relative to the ω motor (motor 0) which rotates the crystal around a horizontal axis normal to the X-ray beam. These two motors move in conjunction to cause precession of the crystal. At the instant depicted here, the crystal alignment axis (dashed line) is tilted up by the precession angle, μ, from the X-ray beam. Precession will cause the projection of the alignment axis on the detector to move in a circle (dashed circle) which at each instant defines the center of the zero circle.

Simulation of a layer-line screen

The second task is to manipulate the display, actually a composite of images collected while the crystal is precessed, to eliminate reflections from reciprocal space layers other than the zero layer. On a conventional precession camera this is accomplished by the physical masking of a moving layer-line screen. This screen has a transparent annulus that is mechanically synchronized with the precession motion of the crystal to allow the reflections from a single layer to pass through the screen and then be recorded on a piece of film, which also moves in synchronization with the crystal. In order to adapt these functions to the area detector equipment, it became apparent that the filtering action of the layer-line screen could be simulated by calculating the active surface of the detector needed to measure only the 'zero circle' reflections and discard the rest (see Fig. 2*b*).

The detector by necessity is fixed on a stationary mount that is adjusted to be normal to the X-ray beam, similar to Buerger's Mark I prototype camera (Buerger, 1964, p. 6). Since the detector does not tilt to be normal to the precession axis, the 'zero circle' is actually an ellipse rather than a circle. However, at precession angles less than 10°, the difference between the major and minor axes of this ellipse is less than 3%. Therefore, in practice, a circular filter (annulus) is calculated with a width large enough to compensate for its approximation to the ellipse and also to accommodate minor misalignment of the crystal up an angular error of 0·1°. The coordinates for the center of this annulus are a function of the incrementing angle variable, n, and were expressed in the previous section as Δx and Δy relative to the direct-beam intersection with the detector. Once the center of the annulus is determined, the active portion of the detector is selected as the area between

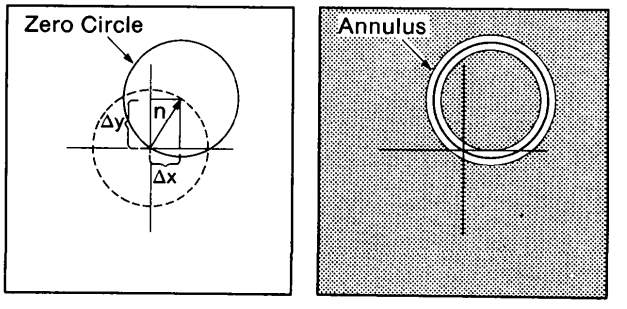

Fig. 2. (*a*) The dashed circle is the projection of the alignment axis on the detector surface as the crystal precesses. Progress along the circle is indicated by a vector drawn from the direct beam to the circle after $n/360$ steps into the precession cycle. It always defines the center of the zero circle. The precession cycle starts at a vertical, 'straight-up' position and proceeds clockwise. Part (*b*), drawn at the same instant as (*a*), shows the electronic masking effect; only the detector elements inside the annulus are active for measurement while the shaded area is temporarily inactive.

two concentric circles, one slightly smaller than the radius of the zero circle ($R = D \tan \mu$) and the other slightly larger (see Fig. 2*b*). All scattered X-rays, reflections and background outside the boundaries of the circular filter are not recorded and therefore do not contribute to the final composite display. This approach has proved to be quite adequate for use with a stationary detector and the resulting display does indeed resemble a conventional precession photograph. We note that a similar approach has been recently used to simulate screened oscillation photography with a Nicolet Imaging Proportional Counter and this has also been useful in the determination of space groups (Gilliland, Howard, Winborne, Poulos, Stewart & Durham, 1987).

Applications

The simulated precession method has been in common use at the University of California, San Diego (UCSD), multiwire area detector facility for four years. We describe two typical applications of its usefulness: the determination of a crystal space group and the evalution of a heavy-atom derivative.

Crystals of anthranilate phosphoribosyltransferase from the bacterium *Erwinia carotovora* were grown by one of us (SLE, details to be presented elsewhere) from a protein sample supplied by Dr Stanley Mills. Grown in a solution of ammonium sulfate and glycerol at 275 K, these cubic-shaped crystals are extremely sensitive to temperature and attempts to determine their space group with a conventional precession camera at room temperature failed. We therefore attempted to determine the space group using the Mark II multiwire area detector equipped with a low-temperature device. A crystal was mounted in a glass capillary and manually adjusted on the goniostat so that the X-ray beam would strike normal to one of its faces. An electronic image resulting from 10 s of X-ray exposure revealed a zero circle which indicated that an axis was nearly aligned with the X-ray beam. After identifying a number of reflections that belonged to the zero circle, a subroutine was invoked to calculate the required motor movements to make the circle disappear behind the beam stop. Further trial and error adjustments of the ω, φ and χ settings caused reflections related by horizontal and vertical symmetry mirrors to appear with nearly equal intensity which usually indicates that the motor values are within 0·1° of true alignment. An initial 3° *screenless* precession image was collected which showed reflections from upper layers besides the zero layer. Subsequently, a 5° simulated screened precession exposure was collected which is displayed in Fig. 3. The total time for image collection and processing was 8 min. Comparison of the screened display with the screenless one indicated that every other reflection was missing in the zero layer. The crystal was then rotated by 90° around the horizontal axis (motor 3) and another precession exposure produced a pattern identical to the previous display,

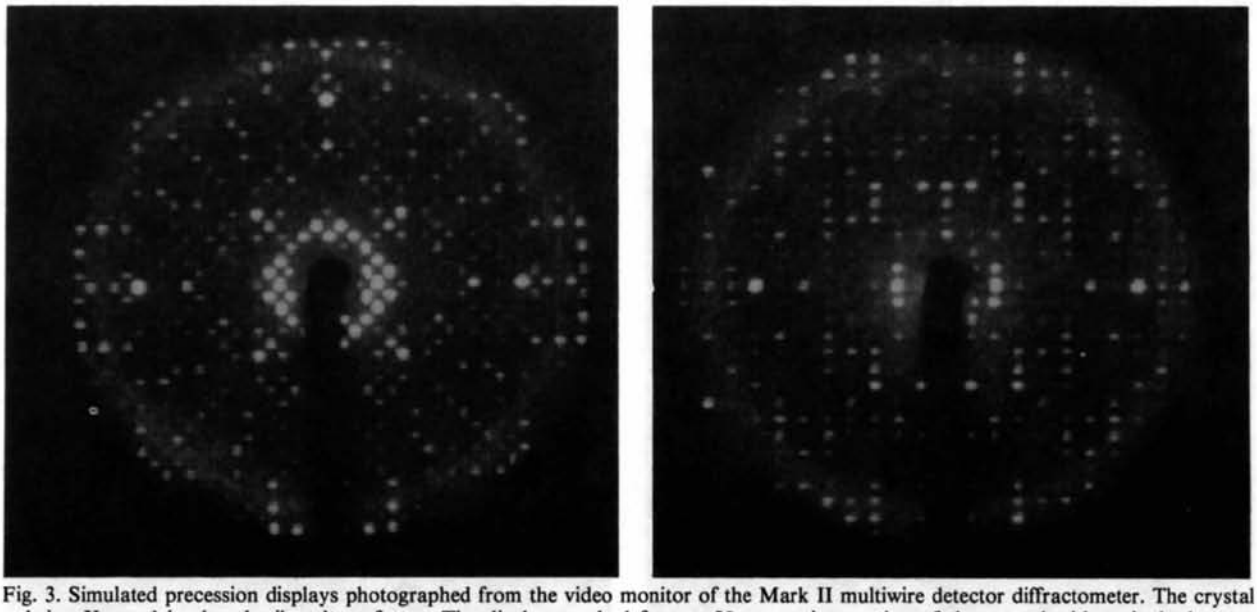

Fig. 3. Simulated precession displays photographed from the video monitor of the Mark II multiwire detector diffractometer. The crystal being X-rayed is phosphoribosyltransferase. The display resulted from a 5° precession motion of the crystal with a single detector positioned 587 mm directly behind the crystal, normal to the X-ray beam. The total time for collecting the 360 images and presenting the final display was 8 min. The left display shows the fourfold symmetry associated with all three axes of the cubic space group. Every other reflection is missing in this projection suggesting body or face centering in the cell. The display on the right shows the result of precessing the 110 axis (with the $1\bar{1}0$ axis vertical and the *c* axis horizontal). Since the reflections are lined up columns, the most likely space group is *I*432.

with fourfold symmetry, from which we were able to eliminate all possible space groups allowed for proteins except $I432$ and $F432$. We then rotated the crystal by 45° around the horizontal axis to bring the 110 axis along the X-ray beam. The resulting display showed all of the reflections arranged in columns with every other column missing. This pattern matched the systematic absences required by $I432$ but not $F432$. The suggested space group, $I432$, has 48 asymmetric units each containing one homodimer. The unit-cell dimensions are $a = b = c = 188$ (1) Å.

The second application is evaluating heavy-atom derivatives of protein crystals for the purpose of determining phases. Simulated precession images from parent and heavy-atom derivatives can be compared visually to detect reflection intensity changes due to the addition of a heavy atom. Although this method can be used to evaluate potential heavy-atom derivatives from a series of experimental trials, it is more commonly used to verify the quality of a known derivative just prior to actual data collection with the area detector. This was the case for data collected at UCSD from crystals of leucine amino peptidase purified from bovine eye lens. Peter David and Eric Gouaux from Professor William Lipscomb's laboratory at Harvard University brought crystals to the UCSD research resource facility for parent and derivative data collection. The derivative was prepared by soaking parent crystals in a solution containing K_2IrCl_6. Photographs of simulated precession images of the parent and the derivative are shown in Fig. 4. The changes in the relative intensities of many reflections due to the heavy atom are obvious and in addition they match the changes expected from conventional precession photographs. Data from these two crystals were collected and are being applied toward solution of the structure.

Future modifications

The simulated precession method as described so far is a very useful substitute for the mechanical precession camera in normal applications. However, we are also investigating possibilities to use the information of the electronic precession image for more sophisticated purposes. For instance, since the images are already digitized, it is possible to apply appropriate background, Lorentz and polarization corrections to extract intensities for indexed reflections. If a heavy-atom derivative is to be compared to a parent image, the intensities from both crystals could be scaled together and the differences plotted as a function of resolution. This would tell the data collector the resolution limit of phasing quality to be expected from a derivative crystal before data collection is begun. In addition, if the intensity differences between parent and derivative can be measured very accurately, it may be possible to calculate a two-dimensional difference Patterson function on demand. The usefulness of such a Patterson has been investigated by Dr Charles D. Stout using a two-dimensional subset of data extracted from two complete sets of parent and heavy-atom-derivative data measured at the UCSD facility. His results indicate that the difference Patterson could be informative under extremely good circumstances – high occupancy of a single site in a medium- to small-sized protein. A major problem is that a difference Patterson map based on the limited number of terms available from a 10°

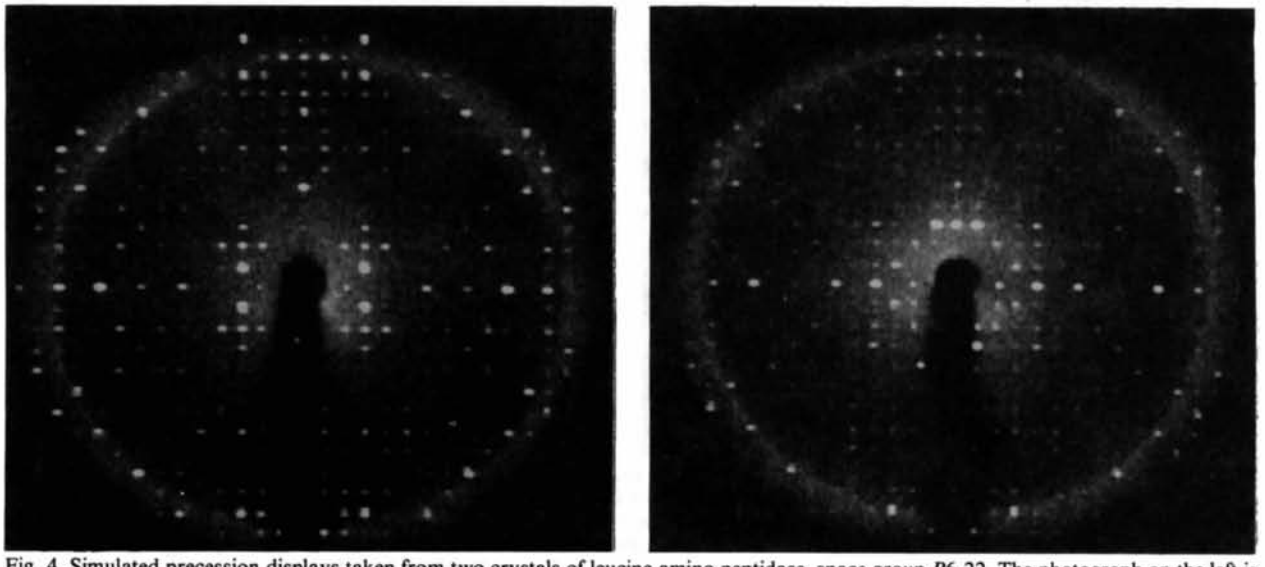

Fig. 4. Simulated precession displays taken from two crystals of leucine amino peptidase, space group $P6_322$. The photograph on the left is from a parent crystal and the one on the right is a heavy-atom derivative. Visual comparison of the two displays confirmed to the operators that the derivative crystal produced the intensity changes expected. (Photographs courtesy of Peter David and Eric Gouaux.)

precession display suffers from ripples caused by series termination effects. However, if a precession angle of 15° were practical, this would allow the use of terms up to a resolution of 3 Å which would result in map of much higher quality. We are exploring modifications necessary to make this feasible.

The real virtue of this electronic precession method is the rapid display, measurement and indexing of selected reflections with a reasonable allowance for crystal misalignment. Simulated precession images are displayed after 5 to 10 min of exposure. This allows the data collector to make a more informed judgement about the nature of a crystal, especially when heavy-atom derivatives are involved, before deciding to proceed with actual data collection. An occasional problem is the difficulty of finding a major axis with crystals of irregular morphology. We are investigating methods to align crystals in random orientations with only the benefit of their cell parameters as are other groups (Messerschmidt & Pflugrath, 1987). When this becomes practical, the time required to evaluate a heavy-atom-derivative crystal may approach the time it takes to mount a trial crystal.

We thank Dr Richard E. Marsh at the California Institute of Technology for useful discussions and Dr Charles D. Stout at the Research Institute of Scripps Clinic for calculating the two-dimensional difference Pattersons. We also thank Dr Stanley E. Mills at UCSD for supplying the protein used in this experiment and Peter David at Harvard University for help in photographing the peptidase displays.

References

BUERGER, M. J. (1964). *The Precession Method.* New York: John Wiley.

GILLILAND, G. L., HOWARD, A. J., WINBORNE, E. L., POULOS, T. L., STEWART, D. B. & DURHAM, D. R. (1987). *J. Biol. Chem.* **262**, 4280–4283.

HUBER, R., SCHNEIDER, M., EPP, O., MAYR, I., MESSERSCHMIDT, A., PFLUGRATH, J. & KAYSER, H. (1987). *J. Mol. Biol.* **195**, 423–434.

MESSERSCHMIDT, A. & PFLUGRATH, J. W. (1987). *J. Appl. Cryst.* **20**, 306–315.

POULOS, T. L., FINZEL, B. C. & HOWARD, A. J. (1987). *J. Mol. Biol.* **195**, 687–700.

WASER, J. (1951). *Rev. Sci. Instrum.* **22**, 563–566.

XUONG, NG. H., SULLIVAN, D., NIELSEN, C. & HAMLIN, R. (1985). *Acta Cryst.* B**41**, 267–269.

Acta Cryst. (1988). B**44**, 187–193

Structure of the Naturally Occurring Iridoid Glycosides 3,4-Dihydrounedoside Pentaacetate, $C_{24}H_{32}O_{14}$, and Pulchelloside II Hydrate, $C_{17}H_{26}O_{12}.H_2O$

BY MARIANNA STRUMPEL, JIANG-TSUN CHEN, JÜRGEN BUSCHMANN AND GERHARD RUBAN

Institut für Kristallographie, Freie Universität Berlin, Takustrasse 6, *D*-1000 *Berlin* 33, *Federal Republic of Germany*

(*Received* 10 *June* 1987; *accepted* 16 *November* 1987)

Abstract

3,4-Dihydrounedoside pentaacetate [compound (1)], 6-(acetoxy)octahydrooxireno[4,5]cyclopenta[1,2-*c*]-pyran-2-yl-β-D-glucopyranoside tetraacetate, $C_{24}H_{32}O_{14}$, $M_r = 544{\cdot}51$, orthorhombic, $P2_12_12_1$, D_m (flotation) = 1·3 Mg m^{-3}, $Z = 4$; at room temperature: $a = 34{\cdot}217$ (9), $b = 10{\cdot}822$ (5), $c = 7{\cdot}572$ (3) Å, $V = 2804$ (3) Å^3; at 140 K: $a = 33{\cdot}565$ (11), $b = 10{\cdot}754$ (4), $c = 7{\cdot}540$ (2) Å, $V = 2722$ (3) Å^3, $D_x = 1{\cdot}329$ Mg m^{-3}, Ni-filtered Cu $K\alpha$, $\lambda = 1{\cdot}5418$ Å, $\mu = 9{\cdot}028$ cm^{-1}, $F(000) = 1152$, $R = 0{\cdot}040$ for 1896 observed reflections. In the iridoidal ring system the six-membered ring has a chair conformation and the five-membered ring an envelope conformation. Bridgehead H atoms, an acetoxy group and the epoxy group, all lie on the same side of the five-membered ring. Pulchelloside II hydrate [compound (2)], methyl 1-(β-D-glucopyranosyloxy)-4a,5,6-trihydroxy-7-methyl-1,4a,5,6,7,7a-hexahydrocyclopenta[*c*]pyran-4-carboxylate monohydrate, $C_{17}H_{26}O_{12}.H_2O$, $M_r = 440{\cdot}40$, orthorhombic, $P2_12_12_1$, $D_m = 1{\cdot}4$ Mg m^{-3}, $Z = 4$, $a = 26{\cdot}943$ (6), $b = 9{\cdot}235$ (4), $c = 7{\cdot}902$ (4) Å, $V = 1966$ (2) Å^3, $D_x = 1{\cdot}488$ Mg m^{-3}, Ni-filtered Cu $K\alpha$, $\lambda = 1{\cdot}5418$ Å, $\mu = 10{\cdot}697$ cm^{-1}, $F(000) = 936$ at room temperature, $R = 0{\cdot}035$ for 1921 observed reflections. In the iridoidal ring system the double bond flattens the six-membered ring to an envelope conformation. The non-H substituents and the only bridgehead H atom are all on the same side of the five-membered ring. The presence of the D-glucose ring, a $^4C_1$ chair in both structures, helped to determine the absolute configuration of the molecules.

Introduction

Chemotaxonomic studies are becoming increasingly important in the classification of plants. A charac-

0108-7681/88/020187-07$03.00